nature communications

Article

https://doi.org/10.1038/s41467-025-60265-8

Spatially blocked split CRISPR-Cas12a system for ultra-sensitive and versatile small molecule activation and detection

Received: 29 November 2024

Accepted: 19 May 2025

Published online: 30 May 2025

Check for updates

Hao Hu[1,2,6], Songcheng Guo[2,6], Yiyuan Li[3,6], Kejun Dong[4], Yan Lu[2], Keyi Ye[2], Longjie Li[3] ✉, Xiaoyu Zhou[5] ✉, Liming Cheng[1] ✉ & Xianjin Xiao[1,2] ✉

Detecting small molecules is pivotal across fields like clinical diagnostics, environmental monitoring, and food safety. The CRISPR-Cas12a system, known for its simplicity and sensitivity, offers a promising basis for small molecule detection. However, current CRISPR-based detection methods face challenges, including complex design requirements, high background noise, and limited adaptability to different targets. In our study, we introduce the SBS-Cas system, leveraging a split crRNA mode to induce spatial hindrance on the scaffold strand through molecular binding. This approach prevents the assembly with Cas12a, effectively masking its trans-cleavage activity. By introducing small molecules that competitively bind to the macromolecule, we eliminate this spatial hindrance, activating Cas12a. Our results demonstrate high sensitivity, versatility, and adaptability in small molecule detection across multiple reactions, with successful intracellular imaging and responsive fluctuations in complex environments underscoring the system's robustness. This innovative CRISPR-Cas12a-based approach establishes a low-background, highly sensitive platform for small molecule detection. SBS-Cas promises not only to enhance tools for clinical, environmental, and food safety applications but also to advance CRISPR research, providing insights and expanding possibilities in molecular detection science.

Small molecules are typically defined as compounds with a molecular weight of less than 1000 Daltons and relatively simple structures[1,2]. Small molecules present within the human body and its interacting environments have a profound impact on human health and environmental sustainability[3,4]. Abnormal changes in small molecules within the bloodstream, such as glucose, cholesterol, and hormones, are often linked to the onset or progression of various diseases[5–7]. Furthermore, the spatial distribution and concentration dynamics of drug metabolites serve as critical indicators of therapeutic efficacy[8,9]. In the environment, small molecules such as heavy metals in air and soil pose substantial risks to ecological systems and public health, causing potentially irreversible damage[10,11]. In the realm of food safety, residual pesticides and toxins generated from spoilage represent serious health hazards, with the potential to lead to life-threatening outcomes[12,13]. Consequently, the detection and analysis of small molecules hold significant importance across diverse fields,

[1]Department of laboratory medicine, Tongji hospital, Tongji Medical College, Huazhong University of Science and Technology, Wuhan 430030, China. [2]Institute of Reproductive Health, Tongji Medical College, Huazhong University of Science and Technology, Wuhan 430030, China. [3]School of Life Science and Technology, Wuhan Polytechnic University, Wuhan 430023, China. [4]Department of Obstetrics and Gynecology, Union Hospital, Tongji Medical College, Huazhong University of Science and Technology, Wuhan 430022, China. [5]Department of Biomedical Sciences and Tung Biomedical Sciences Centre, City University of Hong Kong, Hong Kong, China. [6]These authors contributed equally: Hao Hu, Songcheng Guo, Yiyuan Li. ✉e-mail: lilongjie@whpu.edu.cn; xzhou74@cityu.edu.hk; Chengliming2002@163.com; xiaoxianjin@hust.edu.cn

including clinical diagnostics, environmental monitoring, and food safety.

Traditional methods for detecting small molecules, such as Gas Chromatography-Mass Spectrometry (GC-MS) and capillary electrophoresis (CE), are both highly sensitive and specific[14,15]. However, these techniques require sophisticated instrumentation and expert handling, making them costly and less accessible[16]. Additionally, they are susceptible to interference from biological matrices, which can lead to inaccuracies in measurements. Enzyme-Linked Immunosorbent Assay (ELISA) offers relatively simpler operation, but its sensitivity is often limited due to a lack of signal amplification[17]. Electrochemical methods provide both sensitivity and operational simplicity, yet their electrode stability and detection selectivity can be significantly affected by environmental factors such as temperature and pH[18]. Consequently, these methods are challenging to apply effectively for detecting small molecules in complex samples. Fluorescence-based detection has garnered significant attention from researchers due to its simplicity, stability, cost-effectiveness, and high sensitivity. Fluorescent biosensors employ aptamers or other molecular recognition elements to detect small molecules, often in combination with amplification techniques such as Loop-Mediated Isothermal Amplification (LAMP), Exponential Amplification Reaction (EXPAR), Rolling Circle Amplification (RCA), and Hybridization Chain Reaction (HCR)[19–22]. Additionally, the integration of enzymes like restriction endonucleases and Exonuclease III further enhances fluorescence signal amplification, thereby improving detection sensitivity[23]. However, the design and synthesis of these DNA reaction networks are complex and costly, increasing the overall system complexity and limiting broader application. Furthermore, these reactions typically require large amounts of primers or templates, which may lead to non-specific amplification, causing high background signals and compromising sensitivity.

Recently, biosensors based on Clustered Regularly Interspaced Short Palindromic Repeats (CRISPR)-Cas12a system have received significant attention. Cas12a complexes a CRISPR RNA (crRNA) to form a ribonucleoprotein complex (RNP)[24]. The system utilizes crRNA to specifically recognize target DNA, generating a fluorescent signal through the trans-cleavage activity of Cas12a[25]. With the simplicity, the flexible programmability, and the powerful signal amplification provided by trans-cleavage activity, the Cas12a system has pioneered a revolutionary advancement in the field of molecular detection. Notably, since the Cas12a system directly responds to DNA, the transduction of recognition signals has become one of the most critical areas of research for non-nucleic acid target detection. Currently, there are three primary interfaces for signal transduction in CRISPR-Cas12a-based small molecule detection: allosteric transcription factors (aTF), antibodies, and aptamers. In aTF-mediated small molecule detection methods, double-stranded DNA (dsDNA) containing a PAM sequence is masked by aTF, blocking crRNA recognition. Upon binding with the target small molecule, aTF undergoes a conformational change, releasing dsDNA and subsequently activating Cas12a[26]. However, this approach requires the construction of a fusion protein between aTF and a cellulose-binding domain, which is then immobilized on microcrystalline cellulose. Zhu et al. developed a approach for small molecule detection based on competitive binding between antigens and antibodies[27]. In this article, the antigen is modified on the spacer sequence, which necessitates optimization of its positioning. Moreover, the design can not fully inhibit crRNA-DNA interactions, leading to relatively high background signals. Signal recognition and transduction based on aptamers are among the most widely used methods[28–30]. In these schemes, the aptamer initially binds to a complementary DNA segment. In the presence of a target small molecule, the aptamer undergoes a conformational shift, exposing a sequence that binds to crRNA. Unfortunately, due to the influence of "breathing effect" and the higher affinity of RNA, this approach also suffers from issues of elevated background noise[31]. It is especially noteworthy that the inherent characteristics of small molecules—such as their limited surface area, lack of structural diversity, poor immunogenicity, and scarcity of epitopes—pose significant challenges for developing aptamer-based transduction interfaces[32]. In summary, while the simplicity and sensitivity of the CRISPR-Cas12a system present a feasible foundation for constructing small molecule detection schemes, issues including complex design, high background noise, and limited target adaptability remain critical challenges that need to be addressed.

Herein, we introduce an ultra-sensitive and universal small molecule activation and detection strategy, the spatially blocked split CRISPR-Cas12a system (SBS-Cas). Previous studies have shown that splitting crRNA into scaffold and spacer segments reains the functional properties of full-length crRNA[33]. In our research, we observe that modifying the 3′ end of the scaffold strand with a small molecule does not interfere with the activation of Cas12a's trans-cleavage activity. However, when a macromolecule binds to the modified small molecule, spatial hindrance from the macromolecule hinders the assembly of the scaffold with Cas12a, thereby fully suppressing Cas12a activity. Building on this, we introduce the target small molecule to competitively bind with the macromolecule, thereby alleviating spatial hindrance and generating a detectable signal. Our interface system offers three distinct advantages over existing approaches: 1. Simplified design: the system requires no complex protein constructs, and the small molecule modification is confined to the 3′ end of the scaffold, eliminating the need for repeated optimization. 2. Low background signal: The spatial hindrance introduced by the macromolecule effectively blocks the assembly of the scaffold with Cas12a, fundamentally suppressing trans-cleavage activity and reducing background noise. 3. Expanded target range: the approach enables the quantitative detection of small molecules through the introduction of molecular interactions and competitive displacement. Not only does it maintain compatibility with certain existing transduction systems, but it also broadens the range of target molecules significantly through various binding reactions. We validate the feasibility and scalability of SBS-Cas for quantitative small molecule detection across several molecular binding modes, including antigen-antibody interactions. By optimizing the detection system and leveraging the low-background advantage, we achieve an impressive detection limit for small molecules (10 nM for biotin, 1 nM for m6A, 20 pM for GSH). In addition, we successfully perform imaging of reduced glutathione within live cells, demonstrating the capability for real-time detection of intracellular molecule of SBS-Cas. Furthermore, we apply the 1nt DNA-extended scaffold strategy to conjugate small molecules onto the extended DNA, reducing the modification complexity while expanding the range of detectable small molecules. In summary, by introducing the phenomenon of spatial hindrance-mediated masking of Cas12a activity within a split crRNA mode, we develop a simplified, and low-background approach for small molecule detection. We believe this strategy not only provides an innovative tool for clinical diagnostics, environmental monitoring, and food safety but also enhances our understanding of the CRISPR-Cas12a system.

Results

Principles of SBS-Cas-mediated small molecule detection

Previous studies indicate that dividing the CRISPR-Cas12a crRNA into scaffold and spacer segments preserves its full functionality. Upon hybridization of the spacer strand with a complementary single- or double-stranded DNA within the system, Cas12a's trans-cleavage activity is activated. On the other hand, the interaction of the scaffold—forming a pseudoknot structure—with the WED, RuvC, and REC2 domains of Cas12a is essential for its activity[34]. Building on this foundation, we propose a approach: modifying the 3′ end of the scaffold

https://doi.org/10.1038/s41467-025-60265-8

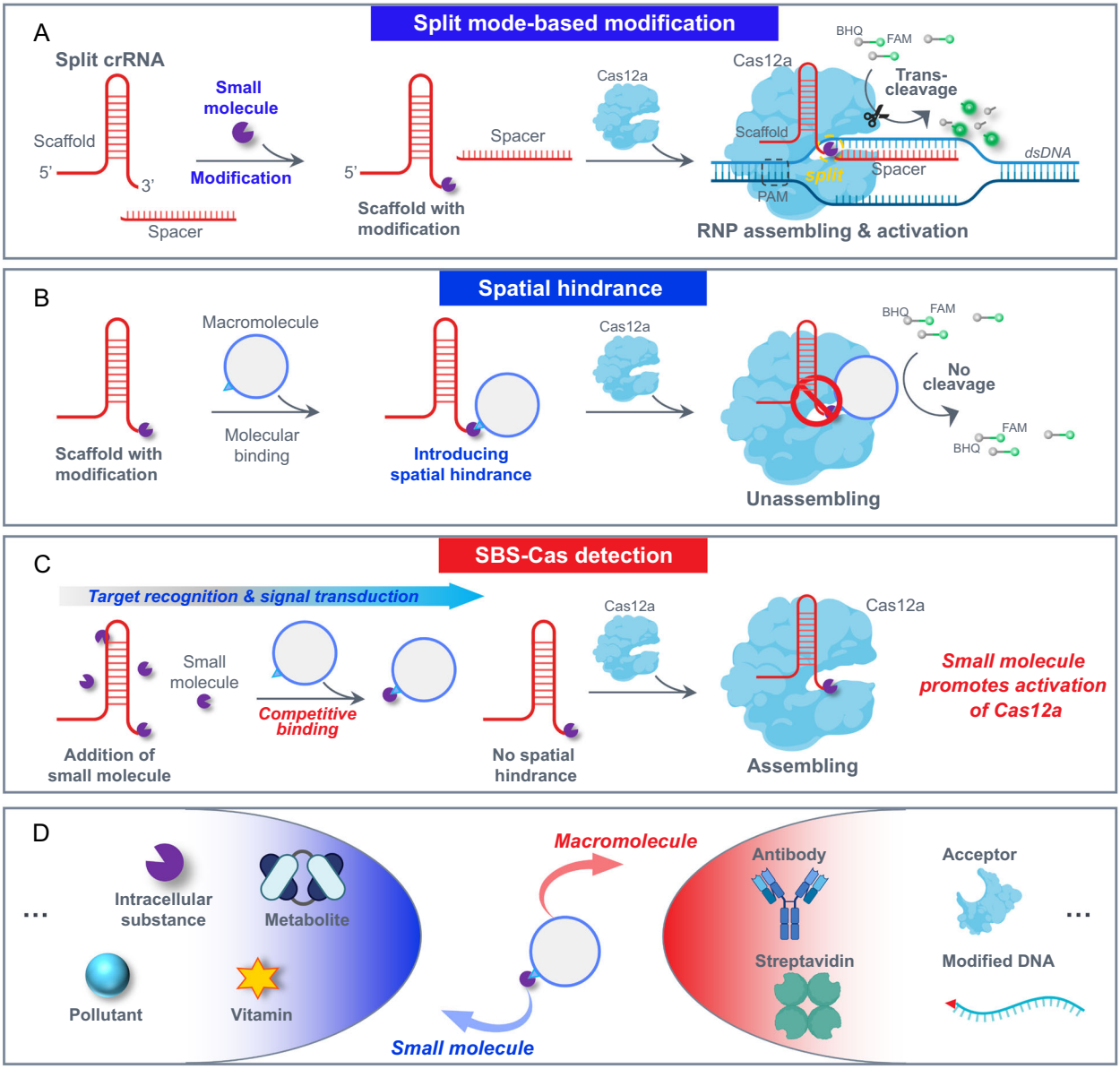


Fig. 1 | The scheme of spatially blocked split CRISPR-Cas12a system. [Created in BioRender. Hu, H. (2025) https://BioRender.com/gzhemn8]. **A** Modification of small molecules at the 3′ end of scaffold does not affect the trans-cleavage activity of Cas12a. **B** Macromolecules inhibit scaffold assembly with Cas12a through molecular binding reaction. **C** Competitive binding of small molecules to be tested to Macromolecules promote scaffold and Cas12a assembly. **D** Macromolecule and small molecule types of the SBS-Cas system.

with the target small molecule and introducing a macromolecule that binds to it. The modification of small molecule does not interfere with the activation of Cas12a's trans-cleavage activity (Fig. 1A). This macromolecule induces spatial hindrance, disrupting the scaffold's structural alignment with Cas12a domains. As a result, the Cas12a system is unable to assemble into the active ribonucleoprotein complex, effectively masking its trans-cleavage activity and suppressing background signal generation (Fig. 1B). Furthermore, in the presence of free target molecules within the system, these molecules competitively bind to the macromolecule. The competitive binding removes the masking effect, thereby restoring the trans-cleavage activity of Cas12a, which generates a fluorescence signal (Fig. 1C). In summary, this design leverages molecular interactions to recognize small molecules and subsequently transduces the small molecule signal into a fluorescent output by releasing Cas12a inhibition through competitive binding. Overall, the rate of fluorescence signal increase would correlate positively with the concentration of the added small molecule, allowing for the establishment of a quantitative assay based on this relationship. Notably, this design benefits from 3′ end modification, which simplifies modification requirements and eliminates the need to optimize the modification site. More importantly, the molecular binding interaction is not limited to antigen-antibody interactions but can also involve various conjugation reactions, such as click chemistry, significantly broadening the range of detectable small molecules (Fig. 1D). We believe that SBS-Cas offers a straightforward and sensitive approach for the recognition and quantification of diverse small molecules.

Validation of SBS-Cas feasibility by detection of acrylamide

To verify the feasibility of our approach, we employed SBS-Cas to detect acrylamide, a small molecule byproduct formed during the Maillard reaction in food, known for its neurotoxic and reproductive

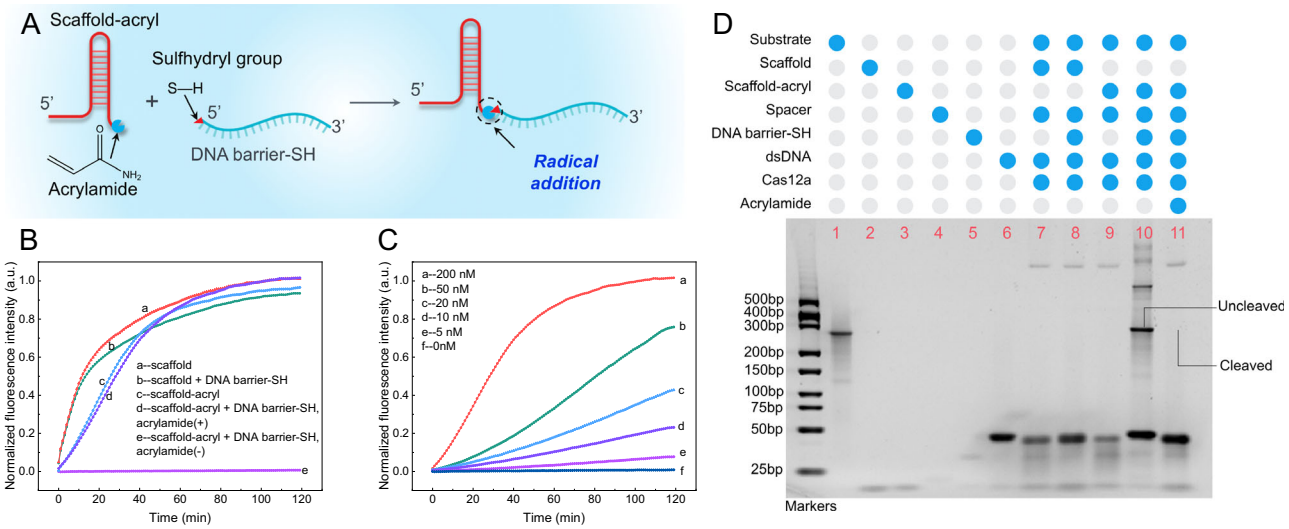
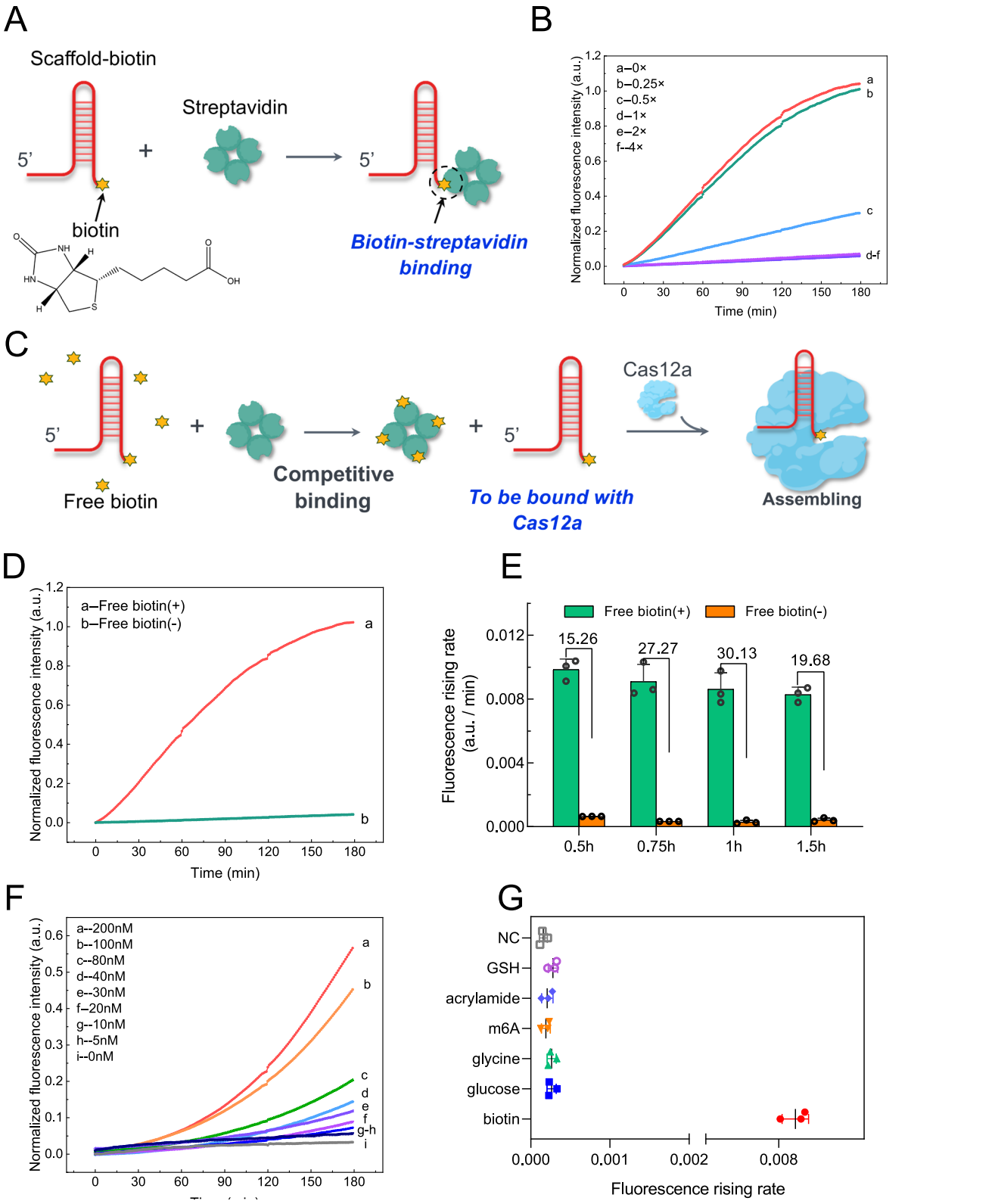


Fig. 2 | SBS-Cas detection of acrylamide based on radical addition reaction. **A** Schematic representation of spatial hindrance introduced by DNA barrier-SH strand binding to scaffold-acryl via radical addition reaction. [Created in BioRender. Hu, H. (2025) https://BioRender.com/gzhemn8]. **B** Fluorescence curves of the Cas12a system of scaffold in the presence and absence of DNA barrier-SH. Fluorescence curves of the Cas12a system of scaffold-acryl, scaffold-acryl with DNA barrier-SH, scaffold-acryl with DNA barrier-SH and acrymide. The final concentrations of the system were Cas12a, 20 nM; scaffold, scaffold-acryl and spacer, 20 nM; DNA barrier-SH, 40 nM; activator dsDNA, 60 nM; acrymide, 200 nM; ssDNA reporter, 100 nM (labeled with FAM and BHQ-1). Cas12a: scaffold/scaffold-acryl/spacer: DNA barrier-SH = 1: 1: 2. There was no dosage relationship between the other components. Reaction condition: 37 °C, 50 µL, 50 mM NaCl, 10 mM Tris-HCl, 14 mM $MgCl_2$, 100 µg/ml recombinant albumin. The competitive binding incubation time was 60 min (including 5 min of ultraviolet irradiation). **C** Rise in fluorescence of SBS-Cas after addition of different concentrations of acrylamide. The final concentrations of added acrylamide were 0 nM, 5 nM, 10 nM, 20 nM, 50 nM, and 200 nM. The concentrations of the other components and the reaction conditions were the same as those in **B**. **D** PAGE analysis of the feasibility of SBS-Cas. The cleavage reaction was carried out in a 15 µL system at 37 °C. The concentrations of each component were as follows: substrate strand, 0.5 µM; Cas12a/scaffold/ scaffold-acryl/spacer, 0.2 µM; activator dsDNA, 0.6 µM; DNA barrier-SH, 0.4 µM; acrylamide, 2 µM. Lanes 1-11 from left to right: Lane 1: substrate strand, a 150nt-ssDNA was used as the substrate to visualize the results; Lane 2: scaffold; Lane 3: scaffold-acryl; Lane 4: spacer; Lane 5: DNA barrier-SH; Lane 6: activator dsDNA; Lane 7:Cas12a + scaffold + dsDNA + spacer + substrate; Lane 8: Cas12a + scaffold + dsDNA + spacer + substrate + DNA barrier-SH; Lane 9: Cas12a + scaffold-acryl + dsDNA + spacer + substrate; Lane 10: Cas12a + scaffold-acryl + dsDNA + spacer + substrate + DNA barrier-SH; Lane 11: Cas12a + scaffold-acryl + dsDNA + spacer + substrate + DNA barrier-SH + acrylamide. The experiment was independently repeated three times with similar results. Source data are provided as a Source Data file.

toxicity effects[35]. We first synthesized a 20-nt RNA sequence to serve as the spacer and utilized a single-stranded DNA fluorescent probe labeled with the fluorophore FAM and quencher BHQ1 at each end as the reporter (Supplementary Table 1). Furthermore, we synthesized both the scaffold strand and the scaffold-acryl strand, with the latter modified at the 3′ end with acrylamide (Supplementary Table 1). Additionally, we synthesized another 20-nucleotide DNA strand with sulfhydryl groups (-SH) at its 5′ end, referred to as DNA barrier-SH (Supplementary Table 1). Under conditions with a photoinitiator and UV light, sulfhydryl groups are capable of adding across the double bonds of acrylamide[36]. The DNA barrier-SH was conjugated to scaffold-acryl, thereby preventing its assembly with Cas12a (Fig. 2A). We first compared the effects of scaffold and scaffold-acryl on trans-cleavage activity with and without the addition of DNA barrier-SH. As shown in Fig. 2B, fluorescence increased in the absence of the barrier strand, demonstrating the validity of the split crRNA mode and confirming that small molecule modification alone does not inhibit Cas12a activity. Upon adding DNA barrier-SH, fluorescence in the scaffold-acryl group showed minimal increase, while the trans-cleavage activity of the scaffold group remained unaffected. This outcome demonstrates the feasibility of the spatial hindrance-mediated masking strategy for CRISPR-Cas12a. Next, we introduced free acrylamide into the system to incubate with scaffold-acryl and the barrier strand. Results showed that acrylamide competitively bound with the barrier strand, thereby removing its inhibitory effect (Fig. 2B). Additionally, the rate of fluorescence increase was concentration-dependent (Fig. 2C), providing a basis for the quantitative determination of small molecule concentrations. This part of the experiment was used to demonstrate whether the principle is feasible and whether the reaction results correlate with the concentration of the substance to be measured. Conditions such as incubation time and DNA barrier-SH were not optimised. In addition to the fluorescence experiments, we conducted polyacrylamide gel electrophoresis (PAGE) to further validate the feasibility of our proposed SBS-Cas (Fig. 2D). In Lane 1, a 150-nt single-stranded DNA (ssDNA) was introduced as the substrate to visualize the trans-cleavage activity. We believe that the primary band appearing around 300 bp is likely due to intermolecular interactions between long single-stranded nucleic acids, leading to the formation of higher-order structures. Additionally, the heterogeneous nature of these aggregated products may have contributed to the observed signs of tailing and diffusion. As shown in lane 10, when scaffold-acryl was bound to DNA barrier-SH, the long single-stranded substrate remained uncleaved. However, upon the addition of acrylamide, trans-cleavage activity was activated, resulting in substrate degradation. Notably, since both the spacer strand and DNA barrier-SH are short single strands lacking secondary structure (Supplementary Figs. 1 and 2), they were not visible under nucleic acid staining (lane 4 and lane 5). It should be noted that we observed high-molecular-weight bands in lanes 7, 8, 9, and 11. We hypothesize that interactions between various DNA and RNA molecules may have led to the formation of stable double-stranded structures that could not be cleaved by Cas12a. As for lane 10, we believe that the scaffold-acryl and DNA barrier-SH interaction prevented assembly of Cas12a and scaffold strand. The combined scaffold-acryl and DNA barrier-SH remained free in solution, further intensifying the formation of double-stranded structures of varying lengths, which likely led to the observed band shift.

Detection of biotin using biotin-streptavidin binding properties

Biotin, or vitamin B7, plays essential roles in metabolic processes, especially in fatty acid synthesis, amino acid metabolism, and glucose



production[37]. The binding interaction between biotin and streptavidin (SA) is one of the strongest non-covalent interactions found in nature[38]. In this section, we combined the SBS-Cas design with the biotin-SA binding mechanism to develop a quantitative detection system for biotin (Fig. 3A). Based on this approach, we synthesized scaffold-biotin, which features biotin attached to its 3' end. We first evaluated the functionality of scaffold-biotin and its interaction with SA. Scaffold-biotin was incubated with varying concentrations of SA (0×, 0.25×, 0.5×, 1×, 2×, and 4×). As shown in Fig. 3B, in the absence of streptavidin binding, scaffold-biotin could assemble with Cas12a, activating trans-cleavage activity and generating fluorescence. With increasing SA concentrations, the fluorescence signal was progressively suppressed, demonstrating that SA effectively inhibits Cas12a by binding non-covalently to biotin on the scaffold. This inhibitory effect reached saturation at an SA concentration of 1× (Supplementary Fig. 3). Building on this, we introduced free biotin to competitively remove

Fig. 3 | SBS-Cas detection of biotin based on biotin-SA binding. A Schematic representation of spatial hindrance introduced by streptavidin binding to scaffold-biotin via biotin-SA binding. [Created in BioRender. Hu, H. (2025) https://BioRender.com/gzhemn8]. **B** Fluorescence curves after adding different concentrations of SA to the system. The final concentrations of the system were Cas12a, 20 nM; scaffold, scaffold-biotin and spacer, 20 nM; activator dsDNA, 60 nM; ssDNA reporter, 100 nM. Reaction condition: 37 °C, 50 μL, 50 mM NaCl, 10 mM Tris-HCl, 14 mM MgCl2, 100 μg/ml recombinant albumin. The incubation time was 30 min. 1× represents the concentration of 20 nM. The final concentrations of SA were 0×, 0.25×, 0.5×, 1×, 2×, and 4×. **C** Schematic representation of biotin competitively binding SA to promote Cas12a activation. [Created in BioRender. Hu, H. (2025) https://BioRender.com/gzhemn8]. **D** Rise in fluorescence of the system after the addition of free biotin. The basic reaction conditions were consistent with **B**, and the final concentration of free biotin was 1 μM. **E** Optimization of incubation time for competitive binding of free biotin and scaffold-biotin to SA. The incubation times were set to 0.5 h, 0.75 h, 1 h, and 1.5 h. The experiments were conducted in three technical replicates and error bars represent mean ± SD (n = 3). **F** The sensitivity analysis for different concentrations of biotin. **G** The selectivity analysis among GSH, acrylamide, m6A, glycine, glucose,biotin. The final concentration of all small molecules was 1 μM. The experiments were conducted in three technical replicates and error bars represent mean ± SD (n = 3). Source data are provided as a Source Data file.

the inhibition (Fig. 3C). As shown in Fig. 3D, SBS-Cas successfully detected this small molecule. To further optimize the detection protocol, we evaluated the impact of different incubation times (0.5 h, 0.75 h, 1 h, and 1.5 h) on biotin detection. Results indicated that a competitive incubation of 1 hour provided the optimal discrimination (Fig. 3E). Following this straightforward optimization, we assessed the sensitivity and specificity of SBS-Cas for biotin detection. As shown in Fig. 3F and Supplementary Fig. 4, the detection limit was determined to be 10 nM (Supplementary Table 2). It is important to note that due to SA's multivalent binding nature, achieving a continuous and precise adjustment of its concentration is inherently challenging. This characteristic directly impacts the detection performance in the low-concentration range, leading to variations in signal response and reduced consistency in detection sensitivity. Additionally, Fig. 3B, 3D, and 3F, even at high SA concentrations or with sufficient incubation time, a noticeable fluorescence increase was still observed in the absence of free biotin competition. This finding led us to further realize he potential influence of additional physicochemical properties, such as molecular shape and electrostatic potential, on Cas12a activity beyond molecular weight. Additionally, SBS-Cas demonstrated excellent specificity, showing no response to various small-molecule interferents (Fig. 3G).

Antigen-antibody binding-based m6A detection

Introducing spatial hindrance through antigen-antibody binding aligns well with the principle of SBS-Cas. This approach has been reflected in previous Cas12a-based small molecule signal transduction methods. In these studies, an antigen was labeled on the spacer sequence, with the antibody-antigen interaction preventing the spacer from binding to complementary DNA. However, this design could not fully block nucleic acid pairing, resulting in high background signals even in the absence of target small molecules. In our approach, after the antibody binds to the modified scaffold, spatial hindrance effectively prevents the scaffold from accessing the nuclease site (Fig. 4A). In this section, we employed antibodies to detect RNA methylation modification, specifically N6-methyladenosine (m6A). m6A is the most common internal methylation modification in mammalian mRNA, playing a crucial role in mRNA nuclear export, splicing, and translation[39]. Its aberrant expression has significant implications for cellular differentiation, tumor progression, and other critical biological processes[40]. We began by modifying the second-to-last rA at the 3′ end of the scaffold strand to m6A, synthesizing the scaffold-m6A1 strand. Using two different brands of diluents, we diluted the anti-m6A antibody to test its ability to bind scaffold-m6A1 and subsequently mask the trans-cleavage activity of Cas12a. Results showed that scaffold-m6A1 could effectively activate Cas12a. Unfortunately, even without antibody, the addition of different antibody diluents resulted in no fluorescence increase (Supplementary Fig. 5). We hypothesized that certain components within the diluents were incompatible with the CRISPR-Cas12a system. Switching to PBS as the antibody diluent, we found that PBS did not affect Cas12a activity, and that antibodies could effectively suppress Cas12a in a PBS buffer system (Fig. 4B). While we anticipated that modifying only the 3′ end of the scaffold strand would be sufficient to achieve spatial hindrance, m6A presents a unique case as it represents a base alteration on RNA. Therefore, we further modified the scaffold by replacing up to five rA residues in the 3′ end and stem-loop structure with m6A (scaffold-m6A1 through scaffold-m6A5) to examine how different positions affect Cas12a activity and antibody masking efficacy (Fig. 4C). Results showed that scaffold-m6A1 achieved the optimal signal-to-noise ratio, reaching 203.6 (Fig. 4D), primarily due to its effective masking capability. Notably, scaffold-m6A4 even enhanced the trans-cleavage activity of Cas12a in the split mode. Based on these findings with scaffold-m6A1, we further investigated whether m6A could competitively bind the antibody and restore enzymatic activity. Physiologically, our aim is to assess m6A levels on RNA strands, the target m6A is represented by an RNA strand modified with a single m6A site. As shown in Supplementary Fig. 6, the addition of m6A target led to an increase in fluorescence, demonstrating that SBS-Cas can utilize antigen-antibody interactions for detecting. Further optimization was conducted for antibody concentration (0.5×, 1×, 1.5×, and 2×) and incubation time for the antibody with scaffold-m6A1 and m6A (0.5 h, 1 h, and 2 h). Results indicated that the optimal signal-to-noise ratio was achieved at an antibody concentration of 1.5×and an incubation time of 1 h, reaching 84.35 (Fig. 4E). Under these optimized conditions, we evaluated the performance of this method for detecting m6A. The detection limit of SBS-Cas for m6A was determined to be 1 nM (Fig. 4F and Supplementary Fig. 7 and Supplementary Table 3). Additionally, we verified the biosensor's specificity and selectivity by comparing its response to m6A, A, G, C, T, biotin, acrylamide and GSH. As shown in Fig. 4G, the biosensor demonstrated a highly sensitive response to m6A only, indicating reasonable specificity.

Michael addition reaction-assisted strategy for the detection of reduced glutathione

Reduced glutathione (GSH), composed of cysteine, glycine, and glutamic acid, plays a vital role in numerous biological processes[41]. As a critical antioxidant, GSH scavenges free radicals and toxins, thereby protecting essential proteins and maintaining molecular physiological functions[42]. Changes in GSH levels are often associated with specific diseases, such as neurodegenerative disorders, liver diseases, and certain types of cancer[43–45]. Therefore, accurate and sensitive determination of GSH levels is of great importance. The thiol group on GSH can form a stable thioether bond through a Michael addition reaction with maleimide[46]. Based on the SBS-Cas principle and this reaction mechanism, we modified the 3′ end of the scaffold with a thiol group, synthesizing scaffold-SH. Additionally, we synthesized DNA barrier-malei, which is modified with maleimide at the 5′ end and has a sequence identical to DNA barrier-SH. Covalent binding between scaffold-SH and DNA barrier-malei masked Cas12a activity. In the presence of GSH, DNA barrier-malei is competitively bound by GSH, removing the barrier and restoring activity (Fig. 5A). As shown in Fig. 5B, this design enables a rapid and effective response to GSH. Subsequently, we performed experiments with DNA barrier-malei concentrations set to 1×, 1.2×, 1.4×, 1.6×, 1.8×and 2× in order. As shown in Fig. 5C, the highest discrimination of the system was achieved when

https://doi.org/10.1038/s41467-025-60265-8

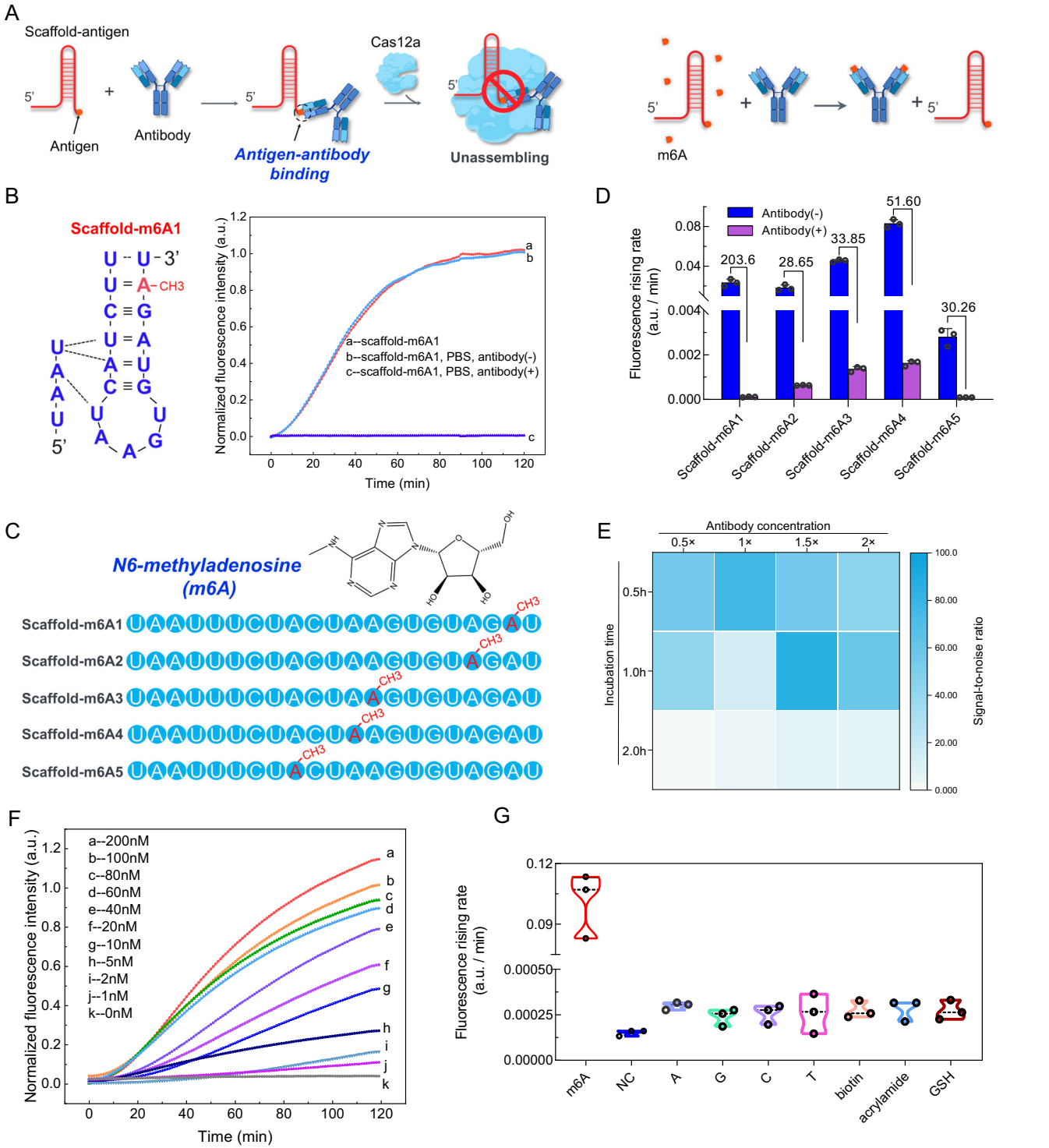
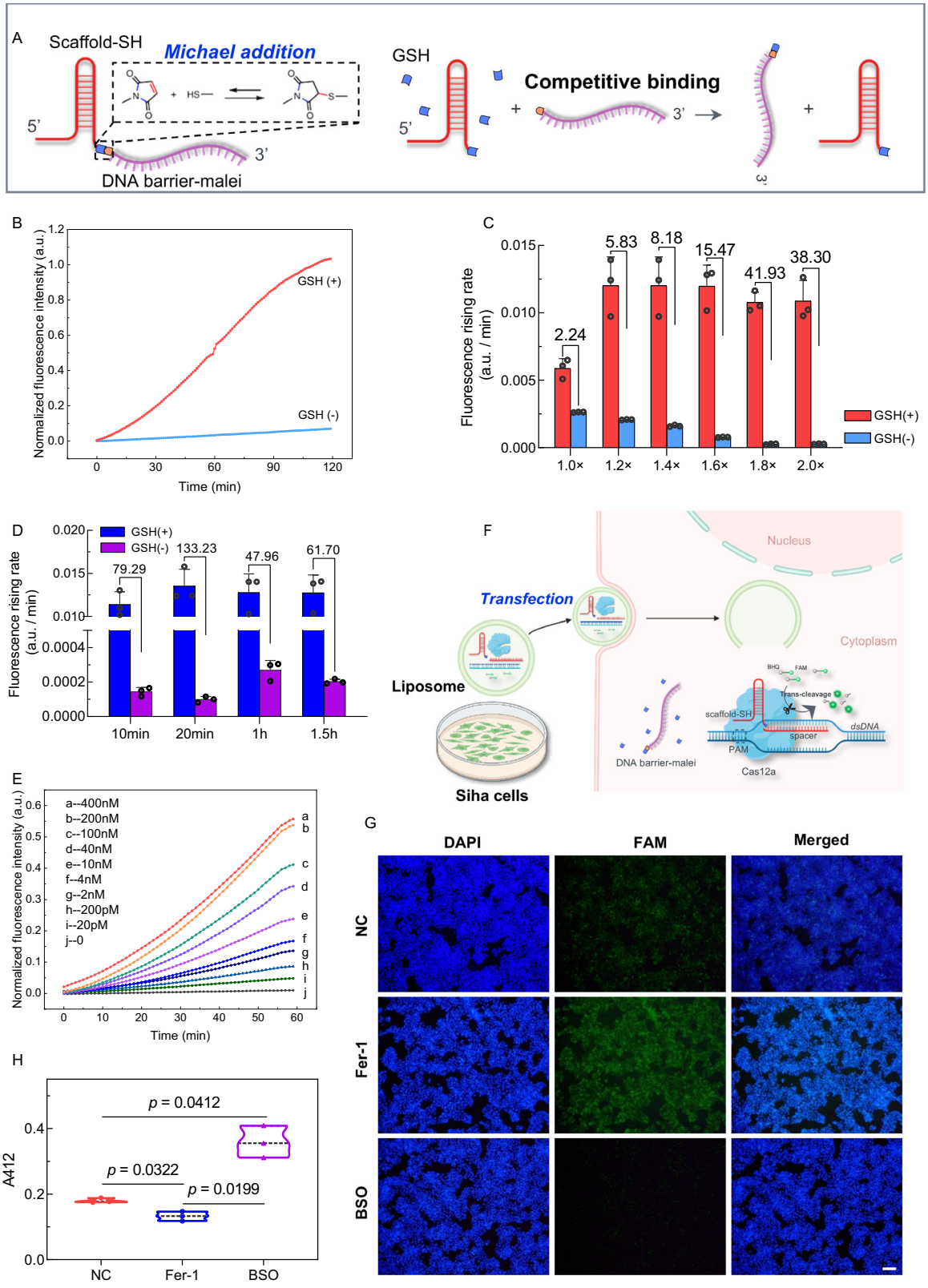


Fig. 4 | SBS-Cas detection of m6A based on antigen-antibody binding. **A** Schematic of SBS-Cas approach based on antigen-antibody binding. [Created in BioRender. Hu, H. (2025) https://BioRender.com/gzhemn8]. **B** Structure of scaffold-m6A1 and inhibition of Cas12a activity by anti-m6A antibody under 1× PBS buffer conditions (pH 7.4). The concentrations of the system were Cas12a, 20 nM; scaffold-m6A1 and spacer, 20 nM; activator dsDNA, 60 nM; antibody 20 nM, ssDNA reporter, 100 nM. Reaction condition: 37 °C, 50 µL, 50 mM NaCl, 10 mM Tris-HCl, 14 mM MgCl2, 100 µg/ml recombinant albumin. The incubation time was 30 min. **C** The m6A structure and the position of m6A in place of rA on the scaffold. **D** Optimization of m6A modification positions on scaffold. The experimental conditions were set as in **B**. The experiments were conducted in three technical replicates and error bars represent mean ± SD (n = 3). **E** Heatmap for optimization of antibody concentration (1× represented 20 nM) and incubation time. The antibody concentration were set to 0.5×, 1×, 1.5× and 2×. The incubation times were set to 0.5 h, 1 h, and 2 h. **F** The sensitivity analysis for different concentrations of m6A. **G** The selectivity analysis among GSH, acrylamide, biotin, A, G, C, T and m6A. The final concentration of all small molecules was 4 µM. The experiments were conducted in three technical replicates and error bars represent mean ± SD (n = 3). Source data are provided as a Source Data file.

https://doi.org/10.1038/s41467-025-60265-8



the concentration was 1.8×. We attribute the high signal-to-noise ratio achieved with the excess DNA barrier-malei strands to their crucial role in spatially hindering scaffold-SH from interacting with Cas12a, thereby effectively preventing the premature activation of trans-cleavage activity. If DNA barrier-malei strands were not in excess, some scaffold-SH would remain unblocked in the absence of GSH, leading to unintended background activation. This background suppression strategy by increasing the concentration of blocking agents has been widely reported in the literature[31,47,48]. Furthermore, DNA barrier-malei strands may exhibit a preferential binding tendency toward GSH. Thus, even under excess conditions, GSH can still effectively disrupt this competitive equilibrium, thereby ensuring transition from "off" to "on" states of the biosensor. The Michael addition reaction proceeds swiftly under ambient conditions without the need for a catalyst. Therefore,

Fig. 5 | SBS-Cas detection of free GSH based on Michael addition reaction. **A** Schematic of SBS-Cas approach based on Michael addition reaction. [Created in BioRender. Hu, H. (2025) https://BioRender.com/gzhemn8]. **B** Rise in fluorescence of the system with and without GSH. The concentrations of the system were Cas12a, 20 nM; scaffold-SH and spacer, 20 nM; activator dsDNA, 60 nM; DNA barrier-malei, 24 nM; GSH, 500 nM; ssDNA reporter, 100 nM. Reaction condition: 37 °C, 50 μL, 50 mM NaCl, 10 mM Tris-HCl, 14 mM MgCl2, 100 μg/ml recombinant albumin. The incubation time was 30 min. **C** Optimization of DNA barrier-malei concentration (1× represented 20 nM). The concentration were set to 1.0×, 1.2×, 1.4×, 1.6×, 1.8×, 2.0×. **D** Optimization of incubation time. The incubation times were set to 10 min, 20 min, 1 h, and 1.5 h. For C-D the experiments were conducted in three technical replicates and error bars represent mean ± SD (n = 3). **E** The sensitivity analysis for different concentrations of GSH. **F** Schematic of GSH intracellular imaging using Liposome-delivered SBS-Cas. [Created in BioRender. Hu, H. (2025) https://BioRender.com/gzhemn8]. **G** Cell fluorescence photo after delivery of SBS-Cas in NC, fer-1-treated and BSO-treated group. The experiment was independently repeated three times with similar results. Scale bar, 50 μm. **H** Relative content of GSSG in NC, fer-1-treated and BSO-treated group. The experiments were conducted in three biological replicates and error bars represent mean ± SD (n = 3). Variance homogeneity was tested using Brown-Forsythe tests. Due to unequal variances (Brown-Forsy $p = 0.0111$), Welch ANOVA was used to assess differences among group means ($p = 0.0092$). Multiple group comparisons were conducted using the Games-Howell post hoc test, which showed significant differences between NC and Fer-1, NC and BSO, and Fer-1 and BSO. Exact p-values are indicated on the figure. Source data are provided as a Source Data file.

we analyzed the fluorescence signal rise rate in the GSH group (GSH(+)) compared to the blank group (GSH(-)) after incubation times of 10 minutes, 20 minutes, 1 hour, and 1.5 hours. Results indicated that a high signal-to-noise ratio was achieved with only 20 minutes of incubation (Fig. 5D). With these optimized conditions in place, we next assessed the analytical performance of the SBS-Cas system for GSH detection. By applying SBS-Cas to samples with varying GSH concentrations, we established a detection limit of 20 pM (Fig. 5E and Supplementary Fig. 8), reflecting two orders of magnitude enhancement in sensitivity compared to existing GSH detection methods (Supplementary Table 4). These results strongly reaffirm that introducing spatial hindrance within the scaffold effectively suppresses background signal, thereby enhancing sensitivity for small molecule detection. Notably, with this approach to spatial hindrance introduction and removal, any test molecule containing a thiol group can competitively bind to DNA barrier-malei to produce a detectable signal. Accordingly, we also investigated the system's response to captopril and dithiothreitol. Results indicated that both small molecules successfully activated trans-cleavage activity (Supplementary Fig. 9).

Intracellular imaging of biomolecules has recently attracted significant interest among researchers. CRISPR-Cas12a-based biosensors have been widely utilized for intracellular imaging of various biomolecules[49–52]. To demonstrate the robustness of our system, we transfected the biosensor into Siha cells using liposomes as carriers. As shown in Fig. 5F, in the presence of intracellular thiol-containing substances, the biosensors delivered into SiHa cells generated green fluorescence. To verify that SBS-Cas can respond to intracellular GSH fluctuations, we prepared three groups of Siha cells. In the first group, we used L-Buthionine-(S,R)-sulfoximine (BSO) to inhibit intracellular γ-glutamylcysteine synthetase, effectively downregulating GSH levels within the cells[53]. In the second group, we added Ferrostatin-1 (Fer-1), a synthetic antioxidant reported to elevate intracellular GSH levels[54]. The third group of cells was left untreated. We then introduced the biosensor into the three groups of cells to observe and compare changes in green fluorescence. As shown in Fig. 5G and Supplementary Fig. 10, the Fer-1 treated group displayed a marked increase in green fluorescence relative to the untreated group, while the BSO-treated group showed a reduction in green fluorescence. Notably, these results were confirmed under consistent DAPI fluorescence intensity across all samples (Supplementary Fig. 11). To further validate that the green fluorescence correlates with GSH levels, we measured oxidized glutathione (GSSG) content using a detection kit. Results showed an increase in GSSG in the BSO-treated group and a decrease in the Fer-1 treated group compared to the untreated control group (Fig. 5H)[55]. It is important to note that the above results only indicate a consistent trend in the upregulation or downregulation of intracellular GSH levels as measured by both methods. However, the exact concentrations were not further quantified. These findings demonstrate that SBS-Cas offers low background signal and high sensitivity. Furthermore, this approach effectively responds to changes in small molecule levels within the complex intracellular environment, enabling intracellular imaging.

Enhancing the feasibility of small molecule detection using the 1nt DNA-extended scaffold strategy

In the above design, the small molecule needs to be modified onto RNA. Given that RNA is prone to degradation, this inevitably increases the complexity of modification and limits its applicability. However, DNA modifications offer greater flexibility, as a wider variety of small molecules can be conjugated to DNA. Additionally, commercial synthesis companies can provide pre-modified deoxyribonucleotide monomers, which expand the range of detectable small molecules while simplifying the method's implementation. Based on this understanding, we extended the 3′ end of the scaffold strand by adding a single deoxyribonucleotide (Fig. 6A), maintaining the fundamental principle of the split crRNA system. We hypothesized that this modified scaffold would still be capable of triggering Cas12a trans-cleavage activity, similar to the unmodified scaffold (Fig. 6B). To validate this, we tested scaffolds extended with one additional nucleotide of adenine (dA), guanine (dG), cytosine (dC), and thymine (dT). The results demonstrated that scaffold+1nt reached a plateau within 90 minutes (Fig. 6C), although single-nucleotide DNA extensions of dG, dC, and dT exhibited a slightly slower activation compared to dA. The variations in activity caused by single deoxynucleotide extensions, along with the results from the biotin detection section prompted us to further investigate the potential influence of additional physicochemical properties, such as molecular shape and electrostatic potential, on Cas12a activity beyond molecular weight. Building upon the 1nt DNA-extended scaffold strategy, we evaluated its feasibility for small molecule detection. Since extending the scaffold with 1nt-A does not affect Cas12a activity, we used scaffold+1nt-A as a platform for further modification with biotin and tested it for biotin detection. As shown in Fig. 6D, scaffold+1nt-A-biotin effectively inhibited Cas12a activity in the presence of SA. Upon introducing free biotin, which competitively binds to SA, a significant fluorescence signal increase was observed. Expanding on this approach, we further applied it to the detection of puromycin, 5-methylcytosine (5mC), and folic acid (Fig. 6E-G). The puromycin and 5mC assays utilized antigen-antibody interactions to mediate signal inhibition and competitive binding, while the folic acid assay employed Folate Receptor Alpha (FOLR1 protein) for specific folic acid binding. In all three cases, the method successfully activated Cas12a trans-cleavage activity. The above results demonstrate that the 1nt DNA-extended scaffold strategy is effective for detecting various small molecules. Since small molecules can be conjugated to DNA, this approach significantly expands the target range and reduces the complexity of preparation.

Discussion

In this study, we leveraged the split crRNA mode to introduce spatial hindrance on the scaffold via molecular binding reactions, thereby preventing its assembly with Cas12a. This design led us to discover a phenomenon in which trans-cleavage activity is effectively masked. By introducing free small molecules to competitively bind with the macromolecule, we removed the spatial hindrance, ultimately developing

https://doi.org/10.1038/s41467-025-60265-8

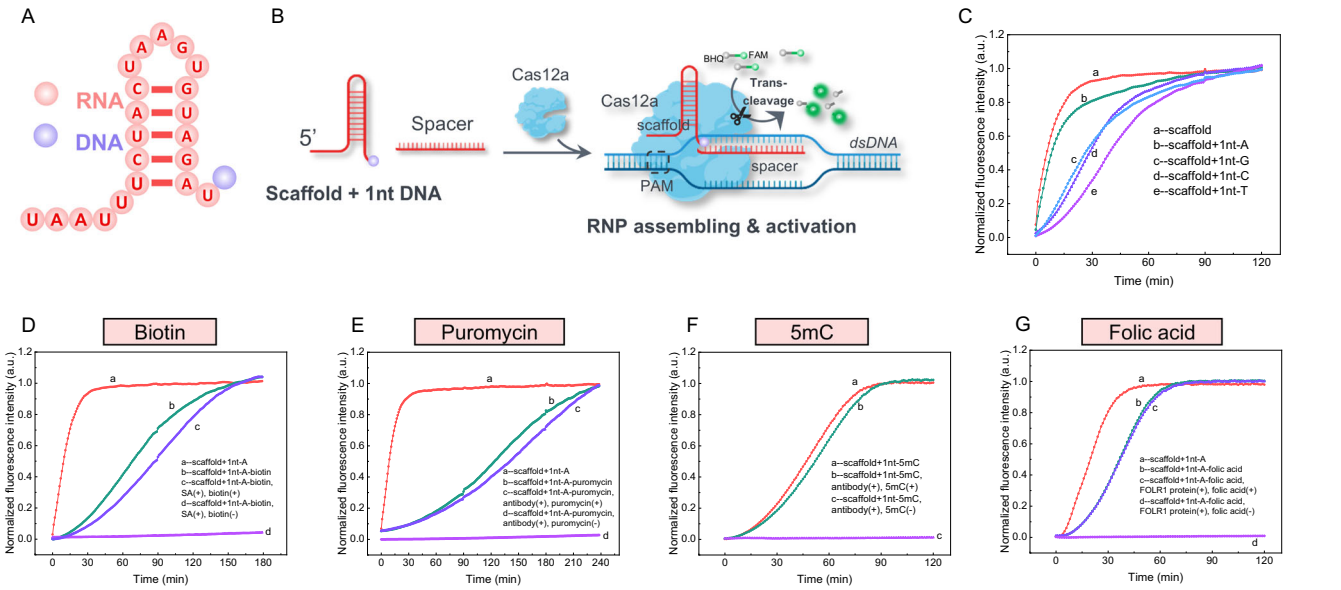


Fig. 6 | Detection of small molecules using the 1nt DNA-extended scaffold strategy. A Schematic representation of the scaffold strand (RNA) extended by a single deoxyribonucleotide (1nt DNA) at the 3′ end. **B** Assembly of the 1nt DNA-extended scaffold strand with Cas12a and subsequent activation of trans-cleavage activity. [Created in BioRender. Hu, H. (2025) https://BioRender.com/gzhemn8]. **C** Fluorescence intensity curves comparing the original scaffold strand with scaffold strands extended by 1nt dA, dT, dC, and dG under identical conditions. The final concentrations in the reaction system were: Cas12a, 20 nM; various scaffold strands and spacer, 20 nM; activator dsDNA, 60 nM; ssDNA reporter, 100 nM. Reaction conditions: 37 °C, 50 μL reaction volume, 50 mM NaCl, 10 mM Tris-HCl, 14 mM $MgCl_2$, and 100 μg/mL recombinant albumin. **D** Biotin detection. Biotin was conjugated to the extended 1nt A on the scaffold strand, with streptavidin (SA) as the macromolecular blocker introducing spatial hindrance. **E** Puromycin detection. Puromycin was conjugated to the extended 1nt A on the scaffold strand, with anti-puromycin antibody serving as the macromolecular blocker. **F** 5-methylcytosine (5mC) detection. Anti-5mC antibody acting as the macromolecular blocker. 5mC nucleotides were incorporated at the 3′ end of the scaffold strand, and a short DNA strand complementary to this scaffold was hybridized (Supplementary Table 1). Under physiological conditions, the target to be revealed is the 5mC level on genomic DNA. Therefore, dsDNA modified with a single 5mC site was used for detection (Supplementary Table 1). **G** Folic acid was conjugated to the extended 1nt A on the scaffold strand, with Folate Receptor Alpha (FOLR1 protein) as the macromolecular blocker. The Cas12a protein and nucleic acid concentrations were identical to those in Fig. 6C. 1× corresponds to 20 nM. The concentrations of SA were set at 1×, antibodies were set at 5×, while FOLR1 protein was set at 2×. The concentrations of the target small molecules were set at 100×. Source data are provided as a Source Data file.

the SBS-Cas system. We demonstrated the feasibility, sensitivity, and target versatility of the SBS-Cas approach by achieving quantitative detection of small molecules across several reactions: radical addition, biotin-streptavidin binding, antigen-antibody binding, receptor-ligand binding and Michael addition. Notably, the detection limit for GSH reached 20 pM, making this approach among the most sensitive currently available for this molecule. Additionally, we successfully performed intracellular imaging of small molecules, with the system's effective response to small molecule fluctuations in complex environments showcasing high robustness of SBS-Cas. Besides, we developed the 1nt DNA-extended scaffold strategy, demonstrating that small molecules can be conjugated to the DNA extension at the 3′ end of the scaffold strand for detection. This approach reduces the modification complexity while expanding the range of detectable small molecules.

Prior to the CRISPR-Cas12a system, small molecule detection was hindered by equipment, workflow, and system complexity. The CRISPR-Cas12a tool, now highly refined, offers a flexible and streamlined approach to molecular detection. This method requires only a fluorescent PCR instrument, making it accessible with minimal equipment and expertise. Originally designed for nucleic acid targets, the CRISPR-Cas12a system has since inspired various interfaces for small molecule recognition and signal transduction. However, existing designs—whether based on aptamer activation or antigen-antibody binding—often face challenges with high background signals. This issue arises primarily from the approach of blocking the crRNA spacer sequence from binding with its complementary DNA, a strategy that often fails to completely inhibit their interaction, allowing even minimal binding events to amplify the trans-cleavage activity. Reducing the background signal in CRISPR/Cas12a-based biosensors is a critical challenge, and several researchers have proposed innovative designs to address this issue. For instance, the Kong group developed an interesting effect termed "RESET", which reduces the number of complementary base pairs between the crRNA and the activator strand, while still maintaining the activator's activation capacity. This strategy makes it easier to block the formation of the Cas12a/crRNA/activator strand complex, thus minimizing background signals[56–58]. Similarly, the Liu group replaced the traditional linear crRNA with circular crRNA in CRISPR/Cas12a-based sensing systems, significantly reducing background noise[59]. The Lee group introduced chimeric DNA-RNA guides, partially replacing the crRNA with DNA to enhance the binding efficiency between crRNA and the activator, thereby reducing non-specific activation[60]. The common goal of these approaches is to suppress the non-specific binding between crRNA and the activator strand from different angles, thereby reducing the background. In contrast, our approach in this work takes a different direction by effectively blocking the assembly of the nuclease with the scaffold, leading to enzyme activity suppression and significantly enhancing the sensitivity of the biosensor.

Our method also has several aspects that require further improvement. It is important to clearly state that the preparation of this method requires the modification of the target small molecule onto the scaffold strand. Although the 1nt DNA-extended scaffold strategy we developed reduces modification complexity, expands the detectable range, and enhances practical applicability, this remains a sticky task, especially for targets lacking active functional groups. Advances in conjugation techniques, such as click chemistry, will be crucial for the further development of this method. In many cases,

conjugating target small molecules to nucleic acids may require optimization of the conjugation process, thereby increasing the overall complexity of the method. The purification steps and their optimization after conjugation are also critical factors that need to be considered, as they directly impact the background signal level. Additionally, effective binding interactions between macromolecules and small molecules are fundamental to the functionality of our approach. While our study demonstrates several binding reactions, identifying suitable macromolecules that can specifically and strongly bind to the small molecule of interest requires effort. Given these unresolved challenges in the field, achieving truly unlimited target adaptability with our method still has a long way to go.

In summary, we have established an innovative CRISPR-Cas12a-based approach that facilitates low-background, highly sensitive, and robust detection across a diverse spectrum of small molecules. This versatile methodology promises not only to provide an enhanced toolset for critical applications in clinical diagnostics, environmental monitoring, and food safety, but also to expand the frontiers of research within CRISPR-Cas systems, offering insights and opportunities for molecular detection science.

Methods

Materials

All DNA oligonucleotide strands used in the experiment were purchased from Sangon Biotech (Shanghai, China). The sequence information was demonstrated in Supplementary Table 1. The purified LbaCas12a, r2.1 buffer, Mg^{2+} were purchased from New England Biolabs (New England, USA). Acrylamide, biotin, RNase-free ddH2O, L-Buthionine-(S,R)-sulfoximine (BSO) were purchased from Sangon Biotech (Shanghai, China). Streptavidin was purchased from Yeasen Biotechnology (Shanghai, China). m6A antibody (68055-1-Ig) was purchased from Proteintech Group (Wuhan, China). Adenine, thymine, guanine, cytosine, captopril, dithiothreitol and glucose monohydrate were purchased from Aladdin Biochemical Technology Co., Ltd (Shanghai, China). Ferrostatin-1 was purchased from MedChemExpress (New Jersey, USA). Captopril and dithiothreitol was purchased from Sangon Biotech (Shanghai, China). Puromycin was purchased from Beyotime Biotechnology (Shanghai, China). Folic acid-PEG-Maleimide (FA-PEG-Mal) was purchased from HWRK chemical (Beijing, China). Anti-puromycin (#MABE343) was purchased from Merck KGaA (Darmstadt, Germany). Irgacure 2959 was purchased from Merck KGaA (Darmstadt, Germany). anti5-mC antibody (68301-1-Ig) was purchased from Proteintech Group (Wuhan, China). Folic acid was purchased from Macklin Biochemical (Shanghai, China). Human FOLR1 Protein was purchased from acrobiosystems (Beijing, China).

SBS-Cas detection assay

The concentration of the oligo-nucleotides was quantified by Nanodrop 2000 (USA). The activator dsDNA for Cas12a was constructed under the progress of heating and annealing. Among the small molecules used in this study, acrylamide, biotin, and GSH were obtained in dry powder form, while puromycin, and folic acid were supplied as solution stocks. Biotin was dissolved in DMSO before use. Acrylamide and GSH were dissolved in ddH_2O before use. These small molecules were diluted to the specified concentrations for use. Cas12a, various scaffold strands, spacer strands were diluted to 1 μM. For the group without target molecules or macromolecular blockers, the reaction mix was prepared as follows: 3 μL Cas12a, 3 μL scaffold strand, 3 μL spacer strand, 1.7 μL NEBuffer r2.1, and 4.3 μL ddH_2O. For the group with only macromolecular blockers binding to the modified scaffold strand, a pre-incubation step was performed by mixing buffer, 3 μL modified scaffold strand, and 3 μL macromolecule. The buffers used were: 1× PBS buffer (pH 7.4) for DNA barrier-malei strands, SA. 20 mM HEPES buffer (pH 7.4) with 50 mM NaCl, 1 mM EDTA and 0.05% (w/v) Irgacure 2959 for DNA barrier-SH. 1× PBS buffer (pH 7.4) with 0.5% BSA and 1 mM Mg^{2+} for m6A antibody and 5-mC antibody. 20 mM HEPES buffer (pH 7.4) with 0.5% BSA for anti-puromycin antibody, and 50 mM tris buffer containing 100 mM glycine (pH 7.5) for FOLR1 protein. For the DNA barrier-SH, the irradiation conditions were set at 365 nm with an intensity of 5 mW/cm². After incubation, the reaction mix was prepared by adding 3 μL Cas12a, pre-incubated mixture, 3 μL spacer strand, 2.7 μL NEBuffer r2.1, and 3.3 μL ddH_2O. For the competitive binding reaction, a pre-incubation step was performed by mixing buffer, 3 μL modified scaffold strand, 3 μL macromolecule, and 3 μL small molecule. To mimic physiological conditions, the actual targets to be detected are m6A or 5mC on nucleic acid strands. In these detections, the targets include m6A or 5mC modifications on strands. After incubation, the reaction mix was prepared by adding 3 μL Cas12a, pre-incubated mixture, 3 μL spacer strand, 2.7 μL NEBuffer r2.1, and 3.3 μL ddH_2O. The incubation time for the competitive binding between the modified scaffold and small molecules with the macromolecule was adjusted according to the optimization experiments. For fluorescence detection, the final system was prepared by adding 5 μL NEBuffer r2.1, 2 μL Mg^{2+} (100 mM), 2 μL reporter strand (2.5 μM), 2 μL activator dsDNA, and reaction mix for different groups. Finally, RNase-free ddH_2O was added to reach a total volume of 50 μL. The pcr tube was then placed in the fluorescent PCR instrument (Bioer Technology Co.,Ltd, China) to measure the fluorescence change. Set the following parameters on to measure fluorescence changes: excitation light wavelength 470 nm, emission light wavelength 535 nm; kinetic interval: 1 min; Gain: 15 (Linegene4840).

Polyacrylamide gel electrophoresis experiment

Prepare 10 mL 12% polyacrylamide gel using TBE buffer. The specific process is as follows: In a clean beaker or tube, mix the following reagents:4 mL of 30% acrylamide/bis-acrylamide solution, 5.9 mL of 10×TBE buffer, 0.10 mL of 10% APS solution. Mix gently, and then add 0.01 mL of TEMED to the solution. Once TEMED is added, quickly pour the solution between the glass plates of the gel apparatus. Allow the gel to polymerize for 30-60 minutes at room temperature. Mix 15 μL of each reaction mix with 3 μL of 6× loading buffer. The oligonucleotide strands were then separated by running the gel at a constant voltage of 110 V for about 90 minutes in 1× TBE buffer. Soak the gel stain (GelRed, Sangon Biotech) solution for 20 minutes after the run, and then wash twice with deionized water. Gel images were taken by Bio-rad Chem-Doc XRS (Bio-Rad, USA).

Cells lines and cell culture

The Siha (cervical cancer) cell lines were purchased by Zhong Qiao Xin Zhou Biotechnology (ZQ0129) (Shanghai, China). They were cultured in DMEM (Gibco) supplemented with 10% FBS (HyClone) at 37 °C in 5% CO2. The culture medium was replaced every 2-3 days, and cells were passaged when they reached 80-90% confluence.

BSO and Fer-1 treatment of Siha cells

Cells were grown in six-well plates in equal amounts per well and left overnight. For the BSO-treated group, 2.6uM pretreatment was given for 24 hours[53]. For Fer-1-treated group, 10uM pretreatment was given to the cells for 24 hours after lysis and dilution according to the instructions of MCE[54].

Assay for GSSG detection

The GSSG level was detected using GSSG assay kit (BTK138, Bioswamp). Wash the cells once with PBS, then centrifuge to collect the cell pellet. Carefully remove the supernatant and add three times the pellet volume of protein removal reagent. Vortex thoroughly to ensure complete mixing. After rapid freeze-thaw cycles, incubate the sample at 4 °C or on ice for 5 minutes. Centrifuge at 10,000 r/min for 10 minutes at 4 °C. Supernatant was collected and incubated with GSH-masking reagents at room temperature for 1 hour. GR and 5,5′-

dithiobis (2-nitrobenzoic acid) were added in the reaction system and kept at room temperature for 5 min, and then the chromogenic reaction was started by adding NADPH. Twenty minutes later, absorbance was analyzed using a microplate reader at 412 nm (Gen5). A more detailed experimental protocol can be accessed at the following website: https://www.bio-swamp.com/goodsDetail/BTK138.

The intracellular imaging

The Siha cells were seeded in a 24-well plate one day before the experiment. Before the transfection, the culture medium was replaced with the medium without serum on the day of operation. We used the liposome as the carrier. The experimental procedure was as follows: a 5 μM solution of scaffold-SH was prepared. For the cell treatment (24-well plate format), 400 μL of culture medium was first added to each well. A mixture was prepared by vortexing 5 μL of scaffold-SH, 0.8 μL of Lipo 8000 (Beyotime, China), and 25 μL of culture medium until fully mixed, which was then added to the wells, and cells were incubated at 37 °C in a 5% CO_2 incubator for 6 hours. Following incubation, the medium was replaced with fresh culture medium. The mixture containing Cas12a (volume: 100 μL) was prepared by combining 1 μL ddH_2O, 20 μL of 25 μM ssDNA Reporter, 25 μL of 15 μM activator dsDNA, 4 μL of 100 mM Mg^{2+}, 10 μL of 10× NEB r2.1 buffer, 10 μL of 45 μM DNA barrier-malei, 20 μL of 12.5 μM Cas12a protein, and 10 μL of 25 μM Spacer strand. Then, 10 μL of the prepared mixture was mixed with 0.8 μL Lipo 8000 and 25 μL of culture medium by thorough pipetting, added to the cells, and incubated at 37 °C for 8 hours before imaging. After incubation washed the cells for three times with the PBS solution. The fluorescent was observed by the microscope (Ningbo shunyu Optical Technology Co., Ltd) under the 470 nm wavelength of the excitation light. The wavelength of excitation light 385 nm/470 nm was used to observe the DAPI/FAM in turn. The exposure of the photos is consistent. For the fluorescence intensity analysis of DAPI and FAM, we used Image J software to analyze under the same threshold.

Preparation of scaffold+1nt-A-folic acid. The scaffold+1nt-A-SH strand was purchased from Sangon Biotech (Shanghai, China). The RNA strand was diluted to a final concentration of 10 μM using 1×PBS buffer (pH 7.2) containing 0.5 mM TCEP and incubated at 25 °C for 30 minutes (50 μL total volume). FA-PEG-Mal was dissolved in a buffer containing 0.1 M sodium phosphate (pH 7.4) and 1 mM EDTA. Subsequently, 50 μL of 50 μM FA-PEG-Mal solution was mixed with the RNA solution and allowed to react for 4 hours at 25 °C in the dark. To remove unreacted FA-PEG-Mal, the reaction mixture was transferred to an ultrafiltration tube with a molecular weight cutoff of 3000 Da (MilliporeSigma) and centrifuged at 12,000 × g. The retained fraction, containing the conjugated scaffold+1nt-A-folic acid product, was resuspended in HEPES buffer (pH 7.4) supplemented with 1 mM EDTA. A second round of ultrafiltration was performed under the same conditions to further purify the conjugated product.

Statistics and reproducibility

Export the fluorescent signal data obtained on the fluorescent PCR instrument to an Excel file, and use ORIGIN software to import the data and draw pictures. Differences were analyzed using GraphPad Prism version 8.0.1. The effect was considered significant if the *P* value was under 0.05 with respect to the control. We normalized the fluorescence results using two reference points: the fluorescence intensity of the system in the absence of activator dsDNA was set as background while the fluorescence intensity produced by Cas12a system with full length crRNA was set as "1" (Cas12a: 20 nM; crRNA: 20 nM; activator dsDNA:60 nM; fluorescent probe: 100 nM). Based on this normalization scale, the fluorescence intensity of each experimental group was subtracted by the fluorescence intensity of the background, and then divided by the fluorescence intensity of the positive control to obtain the normalized fluorescence intensity. No statistical method was used to predetermine sample size, no data were excluded from the analyses, the experiments were not randomized, the Investigators were not blinded to allocation during experiments and outcome assessment. All data generated in this study are provided in Source data file.

Reporting summary

Further information on research design is available in the Nature Portfolio Reporting Summary linked to this article.

Data availability

Source data are provided with this paper.

References

1. Sanford, A. A., Manuel, B. A., Romero-Reyes, M. A. & Heemstra, J. M. Combating small molecule environmental contaminants: detection and sequestration using functional nucleic acids. *Chem. Sci.* **13**, 7670–7684 (2022).
2. Wang, X., Cohen, L., Wang, J. & Walt, D. R. Competitive Immunoassays for the Detection of Small Molecules Using Single Molecule Arrays. *J. Am. Chem. Soc.* **140**, 18132–18139 (2018).
3. Qin, X., Li, H., Zhao, H., Fang, L. & Wang, X. Enhancing healthy aging with small molecules: A mitochondrial perspective. *Med Res. Rev.* **44**, 1904–1922 (2024).
4. Sun, H. et al. In situ monitoring of the selective adsorption mechanism of small environmental pollutant molecules on aptasensor interface by attenuated total reflection surface enhanced infrared absorption spectroscopy (ATR-SEIRAS). *J. Hazard Mater.* **403**, 123953 (2021).
5. Sanders, F. W. & Griffin, J. L. De novo lipogenesis in the liver in health and disease: more than just a shunting yard for glucose. *Biol. Rev. Camb. Philos. Soc.* **91**, 452–468 (2016).
6. Truong, B. et al. Modification of coronary artery disease clinical risk factors by coronary artery disease polygenic risk score. *Med* **5**, 459–468.e453 (2024).
7. Hoffmann, J. P., Liu, J. A., Seddu, K. & Klein, S. L. Sex hormone signaling and regulation of immune function. *Immunity* **56**, 2472–2491 (2023).
8. Ingram, N. et al. Ultrasound-triggered therapeutic microbubbles enhance the efficacy of cytotoxic drugs by increasing circulation and tumor drug accumulation and limiting bioavailability and toxicity in normal tissues. *Theranostics* **10**, 10973–10992 (2020).
9. Lu J., et al. Impact of omega-3 fatty acids on hypertriglyceridemia, lipidomics, and gut microbiome in patients with type 2 diabetes. *Med*, **6**, 100496 (2024).
10. Yang, S. et al. Towards an integrated health risk assessment framework of soil heavy metals pollution: Theoretical basis, conceptual model, and perspectives. *Environ. Pollut.* **316**, 120596 (2023).
11. Dan, S. F., Udoh, E. C. & Wang, Q. Contamination and ecological risk assessment of heavy metals, and relationship with organic matter sources in surface sediments of the Cross River Estuary and nearshore areas. *J. Hazard Mater.* **438**, 129531 (2022).
12. Vu, C. et al. Real-Time Immunosensor for Small-Molecule Monitoring in Industrial Food Processes. *Anal. Chem.* **95**, 7950–7959 (2023).
13. Cai, Z. et al. Correlation between interfacial layer properties and physical stability of food emulsions: current trends, challenges, strategies, and further perspectives. *Adv. Colloid Interface Sci.* **313**, 102863 (2023).
14. Rey-Stolle, F. et al. Low and high resolution gas chromatography-mass spectrometry for untargeted metabolomics: A tutorial. *Anal. Chim. Acta* **1210**, 339043 (2022).
15. Elshamy, Y. S. et al. Nanoflow Sheath Voltage-Free Interfacing of Capillary Electrophoresis and Mass Spectrometry for the Detection of Small Molecules. *Anal. Chem.* **94**, 11329–11336 (2022).

16. Wang, W. et al. Ultrasensitive automatic detection of small molecules by membrane imaging of single molecule assays. *ACS Appl Mater. Interfaces* **14**, 54914–54923 (2022).
17. Wang, Y. et al. Development of a competitive ELISA based on estrogen receptor and weak competitive molecule for the screening of potential estrogens in foods. *Food Chem.* **401**, 134084 (2023).
18. He, J., Spanolios, E., Froehlich, C. E., Wouters, C. L. & Haynes, C. L. Recent Advances in the Development and Characterization of Electrochemical and Electrical Biosensors for Small Molecule Neurotransmitters. *ACS Sens* **8**, 1391–1403 (2023).
19. Yuan, Y. et al. Ultrasensitive electrochemiluminescent aptasensor for ochratoxin A detection with the loop-mediated isothermal amplification. *Anal. Chim. Acta* **811**, 70–75 (2014).
20. Reid, M. S., Le, X. C. & Zhang, H. Exponential Isothermal Amplification of Nucleic Acids and Assays for Proteins, Cells, Small Molecules, and Enzyme Activities: An EXPAR Example. *Angew. Chem. Int Ed. Engl.* **57**, 11856–11866 (2018).
21. Shi, H. et al. The analysis of proteins and small molecules based on sterically tunable nucleic acid hyperbranched rolling circle amplification. *Biosens. Bioelectron.* **91**, 136–142 (2017).
22. Wang, S. et al. Aptasensing a class of small molecules based on split aptamers and hybridization chain reaction-assisted AuNPs nanozyme. *Food Chem.* **401**, 134053 (2023).
23. Cao, J. et al. Harnessing a previously unidentified capability of bacterial allosteric transcription factors for sensing diverse small molecules in vitro. *Sci. Adv.* **4**, eaau4602 (2018).
24. Tian, R. et al. Massively parallel CRISPR off-target detection enables rapid off-target prediction model building. *Med* **4**, 478–492.e476 (2023).
25. Li, S. Y. et al. CRISPR-Cas12a has both cis- and trans-cleavage activities on single-stranded DNA. *Cell Res* **28**, 491–493 (2018).
26. Liang, M. et al. A CRISPR-Cas12a-derived biosensing platform for the highly sensitive detection of diverse small molecules. *Nat. Commun.* **10**, 3672 (2019).
27. Zhu, F. & Zhao, Q. Sensitive CRISPR-Cas12a-Assisted Immunoassay for Small Molecule Detection in Homogeneous Solution. *Anal. Chem.* **95**, 6769–6774 (2023).
28. Ma, L. et al. Sensitive small molecule aptasensing based on hybridization chain reaction and CRISPR/Cas12a Using a Portable 3D-Printed Visualizer. *ACS Sens* **8**, 1076–1084 (2023).
29. Li, X., Chen, X., Mao, M., Peng, C. & Wang, Z. Accelerated CRISPR/Cas12a-based small molecule detection using bivalent aptamer. *Biosens. Bioelectron.* **217**, 114725 (2022).
30. Li Q.-N., et al. Conformational transformation of activator strand directly regulates CRISPR/Cas12a system activity for live cell sensing of multiple biomolecules. *Chem. Eng. J.* **494**, 153084 (2024).
31. Hu, H. et al. Highly-sensitive and homogenous detection of 8-oxoguanine based DNA oxidative damage by a CRISPR-enhanced structure-switching aptamer assay. *Biosens. Bioelectron.* **239**, 115588 (2023).
32. Coonahan, E.-S. et al. Structure-switching aptamer sensors for the specific detection of piperaquine and mefloquine. *Sci. Transl. Med* **13**, eabe1535 (2021).
33. Shebanova, R. et al. Efficient target cleavage by Type V Cas12a effectors programmed with split CRISPR RNA. *Nucleic Acids Res.* **50**, 1162–1173 (2022).
34. Stella, S., Alcon, P. & Montoya, G. Structure of the Cpf1 endonuclease R-loop complex after target DNA cleavage. *Nature* **546**, 559–563 (2017).
35. Yan, F. et al. Acrylamide in food: Occurrence, metabolism, molecular toxicity mechanism and detoxification by phytochemicals. *Food Chem. Toxicol.* **175**, 113696 (2023).
36. Zhu, H. et al. The relationship between thiol-acrylate photopolymerization kinetics and hydrogel mechanics: An improved model incorporating photobleaching and thiol-Michael addition. *J. Mech. Behav. Biomed. Mater.* **88**, 160–169 (2018).
37. Depeint, F., Bruce, W. R., Shangari, N., Mehta, R. & O'Brien, P. J. Mitochondrial function and toxicity: role of the B vitamin family on mitochondrial energy metabolism. *Chem. Biol. Interact.* **163**, 94–112 (2006).
38. Chung, M. C. et al. Affinity-Switchable Interaction of Biotin and Streptavidin for the Signal-ON Detection of Small Molecules. *ACS Sens* **8**, 4226–4232 (2023).
39. Wang, X. et al. N6-methyladenosine-dependent regulation of messenger RNA stability. *Nature* **505**, 117–120 (2014).
40. He, L. et al. Functions of N6-methyladenosine and its role in cancer. *Mol. Cancer* **18**, 176 (2019).
41. Ngamchuea, K., Batchelor-McAuley, C. & Compton, R. G. Rapid method for the quantification of reduced and oxidized glutathione in human plasma and saliva. *Anal. Chem.* **89**, 2901–2908 (2017).
42. Rom, O. et al. Glycine-based treatment ameliorates NAFLD by modulating fatty acid oxidation, glutathione synthesis, and the gut microbiome. *Sci. Transl. Med.* **12**, eaaz2841 (2020).
43. Li, X. et al. The acute effect of different NAD (+) precursors included in the combined metabolic activators. *Free Radic. Biol. Med* **205**, 77–89 (2023).
44. Lu, S. C., Mato, J. M., Espinosa-Diez, C. & Lamas, S. MicroRNA-mediated regulation of glutathione and methionine metabolism and its relevance for liver disease. *Free Radic. Biol. Med* **100**, 66–72 (2016).
45. Koppula, P., Zhuang, L. & Gan, B. Cystine transporter SLC7A11/xCT in cancer: ferroptosis, nutrient dependency, and cancer therapy. *Protein Cell* **12**, 599–620 (2021).
46. Martinez-Jothar, L. et al. Insights into maleimide-thiol conjugation chemistry: Conditions for efficient surface functionalization of nanoparticles for receptor targeting. *J. Control Release* **282**, 101–109 (2018).
47. Lv, Z., Wang, Q. & Yang, M. Multivalent Duplexed-Aptamer networks regulated a CRISPR-Cas12a system for circulating tumor cell detection. *Anal. Chem.* **93**, 12921–12929 (2021).
48. Qiao, B. et al. Aptamer-locker" DNA coupling with CRISPR/Cas12a-guided biosensing for high-efficiency melamine analysis. *Biosens. Bioelectron.* **183**, 113233 (2021).
49. Chen, S. et al. PAM-less conditional DNA substrates leverage trans-cleavage of CRISPR-Cas12a for versatile live-cell biosensing. *Chem. Sci.* **13**, 2011–2020 (2022).
50. Cheng, X. et al. Rapid in situ RNA imaging based on Cas12a thrusting strand displacement reaction. *Nucleic Acids Res.* **51**, e111–e111 (2023).
51. Dong, K. et al. Ultra-sensitive biosensor based on CRISPR-Cas12a and Endo IV coupled DNA hybridization reaction for uracil DNA glycosylase detection and intracellular imaging. *Biosens. Bioelectron.* **226**, 115118 (2023).
52. Wang, X. et al. Dual miRNAs Imaging Platform Based on HRCA-Cas12a by Replacing PAM with Bubble to Reduce False Positive. *Anal. Chem.* **97**, 3053–3062 (2025).
53. Lee, H. R. et al. Adaptive response to GSH depletion and resistance to L-buthionine-(S,R)-sulfoximine: involvement of Nrf2 activation. *Mol. Cell Biochem* **318**, 23–31 (2008).
54. Shao, J., Bai, Z., Zhang, L. & Zhang, F. Ferrostatin-1 alleviates tissue and cell damage in diabetic retinopathy by improving the antioxidant capacity of the Xc(-)-GPX4 system. *Cell Death Discov.* **8**, 426 (2022).
55. Sun, Y. Y. et al. Remote ischemic conditioning attenuates oxidative stress and inflammation via the Nrf2/HO-1 pathway in MCAO mice. *Redox Biol.* **66**, 102852 (2023).

56. Ma, J. Y. et al. RESET" Effect: Random Extending Sequences Enhance the Trans-Cleavage Activity of CRISPR/Cas12a. *Anal. Chem.* **94**, 8050–8057 (2022).
57. Ma J.-Y., et al. CRISPR/Cas12a-based hypochlorous acid and myeloperoxidase biosensors designed on RESET effect. *Sens. Actuat. B: Chem.* **376**, 133000 (2023).
58. Li, Q. N. et al. Low-Background CRISPR/Cas12a sensors for versatile live-cell biosensing. *Anal. Chem.* **95**, 15725–15735 (2023).
59. Wu, Y. et al. Nucleic Acid enzyme-activated CRISPR-Cas12a With Circular CRISPR RNA for Biosensing. *Small* **19**, e2303007 (2023).
60. Kim, H. et al. Enhancement of target specificity of CRISPR-Cas12a by using a chimeric DNA-RNA guide. *Nucleic Acids Res.* **48**, 8601–8616 (2020).

Acknowledgements

X.X. was supported by the National Key Research and Development Program of China [2023YFE0210200] and interdisciplinary research program of HUST. L.L. was supported by the Natural Science Foundation of Wuhan City (Chenguang Project) [2024040801020331]. X.Z. was supported by the central government-guided special funds for local scientific and technological development (no. 226Z2603G), and the Hong Kong Innovation and Technology Fund, the Mainland Hong Kong Joint Funding Scheme (Platform) (No. MHP/240/23). We are grateful to Biorender (https://app.biorender.com/) for offering the online illustration platform.

Author contributions

H.H., S.G. and Y.L. designed the overall research strategy, and coordinated data collection and manuscript writing. X.X., L.C., X.Z., and L.L. were the lead researchers for conceptualization of the project, data analysis and manuscript writing. K.D., Y.L., K.Y. participated in the related experiments. All authors were involved in the preparation of the final manuscript.

Competing interests

The authors declare no competing interests

Additional information

Supplementary information The online version contains supplementary material available at https://doi.org/10.1038/s41467-025-60265-8.

Correspondence and requests for materials should be addressed to Longjie Li, Xiaoyu Zhou, Liming Cheng or Xianjin Xiao.

Peer review information *Nature Communications* thanks Deming Kong, David Walt and the other, anonymous, reviewer(s) for their contribution to the peer review of this work. A peer review file is available.

Reprints and permissions information is available at http://www.nature.com/reprints

Publisher's note Springer Nature remains neutral with regard to jurisdictional claims in published maps and institutional affiliations.

Open Access This article is licensed under a Creative Commons Attribution-NonCommercial-NoDerivatives 4.0 International License, which permits any non-commercial use, sharing, distribution and reproduction in any medium or format, as long as you give appropriate credit to the original author(s) and the source, provide a link to the Creative Commons licence, and indicate if you modified the licensed material. You do not have permission under this licence to share adapted material derived from this article or parts of it. The images or other third party material in this article are included in the article's Creative Commons licence, unless indicated otherwise in a credit line to the material. If material is not included in the article's Creative Commons licence and your intended use is not permitted by statutory regulation or exceeds the permitted use, you will need to obtain permission directly from the copyright holder. To view a copy of this licence, visit http://creativecommons.org/licenses/by-nc-nd/4.0/.

© The Author(s) 2025